Molecular Dynamics Model for Laser Ablation and Desorption of Organic Solids

Leonid V. Zhigilei, Prasad B. S. Kodali, and Barbara J. Garrison*

Department of Chemistry, 152 Davey Laboratory, The Pennsylvania State University, University Park, Pennsylvania 16802

Received: October 31, 1996; In Final Form: January 14, 1997[⊗]

A breathing sphere model is developed for molecular dynamics simulations of laser ablation and desorption of organic solids. An approximate representation of the internal molecular motion permits a significant expansion of the time and length scales of the model and still allows one to reproduce a realistic rate of the vibrational relaxation of excited molecules. We find that the model provides a plausible description of the ablation of molecular films and matrix-assisted laser desorption. An apparent threshold fluence has been found to separate two mechanisms for the ejection of molecules: surface vaporization at low laser fluences and collective ejection or ablation at high fluences. Above threshold the laser-induced high pressure and the explosive homogeneous phase transition lead to the strongly forwarded emission of ablated material and high, from 500 up to 1500 m/s, maximum velocities of the ejected plume expansion. Large analyte molecules get axial acceleration from an expanding plume and move along with the matrix molecules at nearly the same velocities. Big molecular clusters are found to constitute a significant part of the ejected plume at fluences right above the ablation threshold. The processes in the plume are found to have a strong influence on the final velocities of ejected molecules and molecular clusters.

I. Introduction

Laser ablation of organic solids is a process with a wide range of practical applications. In surgery, this process is used for controlled removal of tissue, and scientific and technological efforts are aimed at achieving more precise control over the ablation depth and minimizing thermal and mechanical damage.[1] In mass spectrometry laser ablation is used to produce big nonvolatile organic molecules or ions in the gas phase for subsequent mass-spectrometric investigations.[2] Recent developments of the matrix-assisted laser desorption ionization (MALDI) technique have dramatically increased the available mass range and possible resolution.[3,4] In this situation the molecules of interest (i.e. the analytes) are incorporated into a matrix of molecules that readily absorb the incident laser light.

Despite an active practical use of laser ablation and extensive experimental[5−14] and theoretical[15−22] studies, the understanding of the underlying elementary processes is rather poor and optimum values of the experimental parameters are arrived at empirically. The complexity and diversity of the processes involved in laser ablation, namely, laser excitation of absorbing molecules, energy transfer from the excited molecules into the internal and translational modes of the solid, material disintegration, and prompt forward ejection along with processes in the plume, hinder the analytical description of the phenomenon. Even a qualitative picture of laser ablation has not been established, and analytical models based on such diverse assumptions as the thermofluctuational sublimation of molecules from the surface (surface vaporization)[9,17] and explosive bulk desorption due to a nonequilibrium phase transition[7,16] or critical pressure gradient[14,15,21,22] are used to explain the experimental observations.

In the situation where the analytical description of the laser ablation of organic solids is hindered by the complexity and diversity of the processes involved in the phenomenon, an analysis based on the molecular dynamics (MD) computer simulation technique can provide useful information. The advantage of this approach is that only details of the microscopic interactions need to be specified, and no assumptions are made about the character of the processes under study. The MD method has been extensively used for the analysis of the sputtering processes where desorption is a consequence of momentum transfer in the collision cascade,[23] fast nonequilibrium phase transiton,[24] or high-pressure buildup in the vicinity of the ion track.[25−28] On the other hand, there have been few MD simulations of laser ablation. The differences between ablative photodecomposition and thermal processes in organic polymers have been discussed,[18,19] and preliminary results from MD simulations of micromachining of silicon surfaces by ultrashort laser pulses have been reported recently.[29]

The factors that sufficiently increase computer time consumption and hamper the application of the MD method to the analysis of laser ablation are the relatively long laser pulse times compared to the energy deposition times for ion-induced sputtering and the sufficiently larger number of molecules (and atoms!) involved in the ablation process. Specifically, sputtering has been modeled by $\sim 10^4$ atoms for times $\approx$ 10 ps. Laser ablation has been proposed[3,5] to be a collective phenomenon involving tens of thousands of *molecules* and laser pulse widths of picoseconds to nanoseconds with concomitantly longer ejection times. This system is too large to model by brute force MD methods in terms of both the number of atoms and the time scale required.

There has been an attempt, however, to address the matrix-assisted laser desorption phenomenon by conventional atomic-level MD by Bencsura and Vertes.[20] They have clearly demonstrated both the attractive sides of the MD method and the severe restrictions on the size of the model and the time of the simulation. They explicitly include 202 matrix molecules and one analyte molecule and follow the atomic motions for 45 ps. They were able to follow the dynamics of disruption of the hydrogen bonds due to the instantaneous temperature jump representing the laser pulse. The small size of the model ($\sim$2 nm), however, could certainly have a profound impact on many aspects of the simulated phenomenon and hampers the direct

[⊗] Abstract published in *Advance ACS Abstracts,* March 1, 1997.

S1089-5647(96)03401-3 CCC: $14.00

correlation of predictions with experimental observations. Moreover, the details of the laser pulse characteristics have not been specified.

In the present work we present an approach aimed at overcoming these limitations by extending the time scale and length scale of the MD model for laser ablation. This approach makes use of the fact that molecules in organic solids have a tightly bound internal structure and form a weakly bound external structure.[30] This feature distinguishes molecular solids from other forms of matter and allows one to treat the external and internal molecular motion separately. To account for the finite rate of the vibrational relaxation of excited molecules and still be able to simulate the collective effect of laser ablation, we propose a model of breathing spheres, a model with true translational but approximate internal degrees of freedom. In this model all molecules are represented by spherical particles. The internal molecular motion is represented in a very approximate way, which, however, allows one to reproduce a realistic rate of the conversion of internal energy of the excited molecules to translational motion. This approximation permits a reasonably large number of molecules to be treated in the simulation study and, hence, leads to information about the collective effect of laser ablation. Moreover, since the vibrational motion, especially for light H atoms, is not being followed explicitly, a large time step in the numerical integration can be used.

In the following section we give a detailed description of the proposed breathing sphere model for the laser ablation of organic solids. The model is then applied to the investigation of the laser ablation of molecular films. The computational setup for the simulation of the molecular systems is given in section III. Preliminary results of the MD simulation performed on both two-dimensional (2D) and three-dimensional (3D) versions of the model are presented in section IV. The 2D simulation offers a clear visual picture of the ablation process and helps one to understand the basic ideas about the mechanisms leading to the laser ablation and the subsequent processes in the ejected plume in considerably shorter computer time. The 3D model has the advantage of directly mapping to experimental conditions in which a quantitative comparison between the computed and experimental results can be made. The summary of the work is given in section V.

II. The Model

The microscopic effect of laser irradiation falls into two broad categories: vibrational excitation and photochemical-induced fragmentation. Vibrational excitation can occur with infrared (IR) as well as with ultraviolet (UV) irradiation. In the case of IR irradiation the laser light is resonantly absorbed into OH or NH stretching vibratins.[12] With UV irradiation electronic excitations of molecular chromophores (typically a pyridine ring or another aromatic π-electron system in a matrix molecule) relax by internal conversion[11] to the vibrational excitations of a molecule. Redistribution of intramolecular energy that initially appears in particular vibrational modes of an excited molecule has been found to be fast, within $\sim$1 ps,[31,32] and is followed by a much slower process of cooling of the vibrationally hot molecule. Computer simulations of the process of vibrational cooling give characteristic times of a few tens of picoseconds,[33] which is consistent with the observation of a 20 ps onset for the ablation process.[34] Alternatively, UV light can also photofragment the molecule. In this scenario, the laser energy is expended in breaking chemical bonds and forming molecules with smaller numbers of atoms. The resulting molecules occupy a larger volume and create pressure inside the irradiated volume, which can then convert to translational energy of ablation. The process of energy transfer in this case is considerably faster than vibrational relaxation mentioned previously.[18,19] Both of the possible results of a photon absorption, photofragmentation and vibrational relaxation of an excited molecule, are incorporated in the breathing sphere model described below.

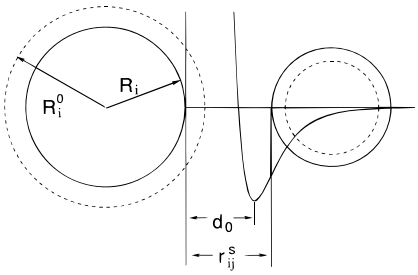

Figure 1. Potential of intermolecular interaction. R_i^0 and R_i are the equilibrium and instantaneous radii of the particle i; d_0 and r_{ij}^s are the equilibrium and instantaneous distances between the edges of the spherical particles.

The effect of the internal excitation of matrix molecules by the laser pulse and the relaxation of the excited molecules are described by a breathing sphere model. Three translational and one internal degree of freedom are attributed to the breathing sphere representing an organic molecule. The Lagrangian, L, that describes the motion in the system of these interacting molecules is given by

$$L = 1/2\sum_i m_i(\mathrm{d}r_i/\mathrm{d}t)^2 - \sum_{ij} U_r + 1/2\sum_i M_i(\mathrm{d}R_i/\mathrm{d}t)^2 - \sum_i U_R \quad (1)$$

where m_i, r_i, and R_i are the mass, position, and radius of the ith molecule, as shown in Figure 1. The inertia or effective mass of the internal motion is denoted by M_i. The potential among the particles is U_r and the internal potential is U_R, both of which are defined below.

The interaction among the organic molecules is assumed to be pairwise additive as

$$U_r = \epsilon_n[\exp\{-2\alpha(r_{ij}^{\ s} - d_0)\} - 2\exp\{-\alpha(r_{ij}^{\ s} - d_0)\}] \quad (2)$$

where $r_{ij}^s = |r_j - r_i| - R_i - R_j$, as shown in Figure 1, with the equilibrium distance d_0 defined as the distance between the edges of the spherical particles rather than their centers. This choice of equilibrium distance is based on the physical concept that the sublimination or cohesive energy of an organic solid is governed primarily by the interaction among atoms on the outside of the molecule. This description allows an easy means of simulating a multicomponent organic solid without introduction of additional specific potentials for different types of organic molecules (i.e. matrix, analyte (big), and photofragmented (small)).

An internal degree of freedom is attributed to each molecule by allowing the spheres representing the organic molecules to change their sizes. The characteristic frequency of the internal motion is controlled by the parameters of the anharmonic potential ascribed to the internal degree of freedom:

$$U_R = k_1\Delta R_i^{\ 2} + k_2\Delta R_i^{\ 3} + k_3\Delta R_i^{\ 4} \quad (3)$$

where $\Delta R_i = R_i - R_i^0$, as shown in Figure 1. The rate of the intermode energy transfer (primarily vibrational) is determined by the size of the anharmonicity and frequency mismatch between vibrational modes.[25,35,36] Thus, the parameters of the internal potential can be used to affect the coupling between

internal molecular motion and phonon modes and to achieve a desired rate of energy transfer from an excited molecule.

The effect of laser irradiation is simulated by vibrational excitation or photofragmentation of random molecules during the time of the laser pulse within the penetration depth. The absorption probability can be modulated by Beer's law[3] to reproduce the exponential attenuation of the laser light with depth. In this case the probability for a given molecule to be excited depends on the fluence of the laser pulse and the position of the molecule under the surface relative to the penetration depth. Vibrational excitation is modeled by depositing a quantum of energy equal to the photon energy into the kinetic energy of internal vibration of a given molecule. In other words, the third term in eq 1 gets a corresponding instantaneous increase. The photofragmentation, when an excited molecule reacts photochemically and forms fragments, can be simulated within the model in two different ways. An instantaneous increase of the *equilibrium* radius of an excited molecule, R_i^0, can be used to represent an increase in the volume occupied by the reaction products.[18,19] This increase of R_i^0 shifts ΔR_i to the repulsive part of the internal potential, eq 3, and creates a local pressure pulse in the vicinity of the excited molecule. The pressure pulse can then dissipate to the thermal energy of the irradiated volume or, at high fluences, convert to the translational energy of ablation.[18,19] An alternative way of simulation of a photofragmentation event is to replace the sphere representing a molecule to be excited with several smaller spheres representing the resulting photofragmented molecules. The advantage of this approach is that the fate of the fragments can be followed during the course of the MD simulation and their role in the ablation process can be analyzed.

III. Computational Setup for the Laser Ablation of Molecular Films

The MD model described above is applied in this work to simulate laser ablation due to vibrational excitations in molecular systems. The parameters of the model chosen for this particular application are given in this section.

A. The sizes of the Model and Boundary Conditions. Two-dimensional simulations have been performed for hexagonal close-packed crystallites of sizes 81 × 210 nm (model A), 81 × 70 nm (model B), and 40 × 35 nm (model C) consisting of 58 800, 19 600, and 4950 matrix molecules, respectively. The smaller model is used primarily for pictorial renditions. For 3D simulations an amorphous molecular solid of dimensions 10 × 10 × 40 nm consisting of 27 648 matrix molecules is used. A smaller amorphous solid was first prepared from a close-packed crystal consisting of 864 molecules. Melting of the crystallite and subsequent quenching from the melt leading to the material amorphization has been simulated using the Andersen−Nose constant-pressure MD technique.[37] The 864 molecule amorphous solid is then replicated to generate the larger computational cell.

Periodic boundary conditions in the direction parallel to the surface are imposed. The bottom molecules are held rigid in the case of the 2D model. More complex boundary conditions at the bottom of the 3D model are discussed later in this section. Periodicity in the direction parallel to the surface simulates the situation in which the radius of the laser beam is large compared to the penetration depth so that the effect of the edges of a laser spot can be neglected. In other words, processes occurring in the center of the laser beam are being examined.

The boundary condition at the bottom of the computational cell can significantly influence the results of the simulations and requires special consideration. The high pressure associated with the ablation process[38,39] generates a pressure pulse that propagates into the surrounding material. The pressure pulse develops into a shock wave that gradually attenuates due to the interaction with the following unloading wave and dissipation into internal energy of material across the shock wave.[38−40] The small size of the MD computational cell does not allow a direct simulation of the attenuation process and inevitably leads to artificial border effects. Rigid boundary conditions, used in 2D simulations, lead to the reflection of the shock wave from the rigid layer and a temporal spike of the compressive pressure in the border region. The reflected shock wave then reaches the surfae and can contribute to the material ejection.[25,27]

In the case of the 2D model, however, we can afford to deal with the problem of the bottom boundary condition by merely increasing of the size of the computational cell. The velocity of propagation of the pressure wave in the 2D model of an organic solid is calculated to be 2760 m/s, and for models A and B it takes respectively about 120 and 40 ps for a pressure wave to cover the distance between the high-pressure region formed within the penetration depth and the rigid layer, to be reflected, and to reach the surface. The processes of the matrix disintegration and ejection are rapid and occur prior to the time in which the surface region is subjected to the reflected shock wave even for the smaller model B. Thus the effects of the ablation and the surface response to the reflected pressure wave are separated in time and can be analyzed independently. Additional testing of the effect of the boundary condition is performed by comparing the results for model B with results for the bigger model A where the surface region does not feel the boundary effects up to 120 ps after the ablation initiation.

In the case of the 3D model we are using a different approach because a further increase of the computational cell is too computationally expensive. In this case we follow the recipes for the reduction of the effects of the reflected shock wave proposed in the MD simulations of sputtering.[24,26,28] In particular, we increase the mass of the molecules in the bottom 8 Å by a factor of 10 and apply the velocity dampening technique, where the velocity of every molecule within the bottom 40 Å is taken to be zero every time the kinetic energy of the molecule maximizes. This condition allows us to minimize the effect of the shock wave reflection and to avoid shock-induced fracturing of the matrix for laser fluences reported in this paper. Prescriptions for accurately damping the shock wave are under investigation.

B. The Potential Parametrization and the Laser Energy Deposition. For the simulations presented in this paper a set of parameters ($d_0 = 3$ Å, $\epsilon_n = 0.1$ eV, $\alpha = 1$ Å^{-1}) have been chosen. For matrix molecules with a mass of 100 Da and an equilibrium radius R_i^0 of 1.4 Å (Figure 1), the predicted properties of a 3D molecular solid are as follows: sublimation energy of 0.6 eV, elastic bulk modulus of ∼5 GPa, density of 1.2 g/cm^{-3}, and phonon spectra with a single broad band centered at 45 cm^{-1} with a width of ∼50 cm^{-1}, as shown in Figure 2. These values are typical for molecular solids.[30]

As mentioned above, the proposed breathing sphere model allows one to easily incorporate other species. In the present work analyte molecules with a mass 20 times that of the matrix molecules and $R_i^0 = 10$ Å are introduced into the 2D model. Each analyte molecule replaces in this case 18 matrix molecules. The positions for eight (model C) or 30 (model B) analyte molecules to be introduced are chosen at random, and the results for five runs with different initial configurations are averaged for model B in order to obtain statistically significant data on the ejection of analyte molecules.

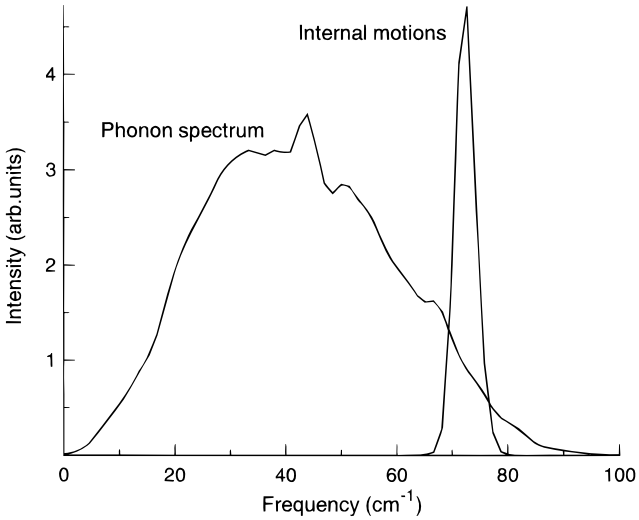

Figure 2. Vibrational spectrum of the 3D model of organic solid calculated at 300 K. Internal molecular motion is represented by one vibrational mode.

For the calculations presented in this paper the parameters of the internal potential ($k_1 = 30$ eV/Å^2, $k_2 = -60$ eV/Å^3, $k_3 = 60$ eV/Å^4, and the inertia parameter M equal to 5000 and 3200 Da in 2D and 3D simulations, respectively) are chosen to provide the characteristic time of the cooling of an excited molecule to be on the order of 10 ps.[33] The spectral peak corresponding to the internal vibrations in this case is embedded into the high-frequency tail of the phonon spectrum as shown in Figure 2 for the 3D system.

The laser irradiation in the present work is simulated by vibrational excitation of random matrix molecules. The total number of photons entering the model solid during the laser pulse is determined from the laser power and the pulse width. In the 2D model the absorption probability is evenly distributed over a penetration depth of 32 nm. The results of the 3D simulation are used for qualitative comparisons with experimental data, and the exponential decrease of the absorption probability with depth is simulated in accordance with Beer's law. A penetration depth of 7 nm is used in this case in order to provide an absorption of 99% of the laser energy within the computational cell. Laser pulses of 15 ps in duration at a wavelength of 337 nm (3.68 eV) are used in the simulations. The photon energy is scaled down by a factor of 2 for the 2D model in order to account for the lower cohesive energy of molecules in the 2D crystallite as compared to the 3D case. Note that in the case of UV irradiation an excited molecule can break up and form fragments. The role of photofragmentation under conditions typical for UV-MALDI experiments is not firmly established, but it is typically believed not to be dominant.[11] Thus, while the model allows us to account for photofragmentation processes, as discussed in section II, this has not been done in the present work. The characterization of the ablation process driven by the photofragmentation of excited molecules is a subject of our current study.

C. Analysis of Simulation Results. The MD simulation technique allows one to perform a detailed analysis of the laser ablation processes in which macroscopic parameters of the system can be correlated with data on microscopic dynamics at the molecular level. Velocity, angle, and ablated cluster distributions can be calculated for both matrix and analyte molecules. These characteristics are closely related with the quality of the mass spectra and can be directly compared with experimental observations. At the same time a number of local physical characteristics are used to describe the system at the molecular level. The energies and velocities of molecules are obtained directly from the MD algorithm. The Dirichlet construction[41] has been used to define the volume per molecule or local density and the coordination number of each molecule in the 2D model. The coordination numbers are conventionally used for characterization of the defect structure of 2D systems.[41−43] All varieties of structural defects in 2D crystals can be identified in terms of groups of non-6-fold coordinated particles,[41,42] and the melting corresponds to the rapid increase of the defect density.[41,43] Thus, calculation of the number of non-6-fold coordinated molecules can provide a quantitative description for the structural changes and phase transitions occurring in the 2D model. To calculate pressure at the location of a molecule, the concept of local atomic stresses commonly used in computational material science[44] has been extended for these molecular interactions, and the local hydrodynamic pressure is defined as a first invariant of the stress tensor. The vibrational spectra (Figure 2) are computed by taking the Fourier transform of the velocity−velocity autocorrelation functions.[36]

A Nordsieck predictor−corrector algorithm is used to integrate the equations of motion.[45] The largest simulation performed here is ∼60 000 molecules for 1 ns at a time step of 5 fs. This simulation required ∼1 CPU hour on an IBM RISC 6000 computer for each 1 ps of molecular motion. A typical matrix molecule (e.g. cinnamic acid) has 19 atoms. To follow H atom vibrational motion, a time step of ∼0.1 fs must be used. If explicit atoms were included in this simulation, the computer time would increase by a factor of $\sim 10^3$. Since each simulation for the breathing spheres already takes several days, including explicit atoms would be computationally prohibitive.

IV. Results and Discussion

In this section we present the results of the MD simulation of the laser ablation of molecular systems. These results demonstrate the capabilities of the breathing sphere model and provide insight into the fundamental processes involved in the ablation phenomenon. First, based on the results of the 2D simulation, a qualitative analysis of the processes and mechanisms leading to the matrix disintegration and collective ejection is presented. The processes in the ejected plume and the ejection parameters of big analyte molecules incorporated into a matrix are then discussed. Finally, preliminary results obtained for the 3D model are used to support the conclusions based on the 2D simulation and to make direct comparisons with experimental results.

We start with a discussion of the results of the 2D simulation for laser irradiation of 15 ps pulse duration. For this discussion we have chosen a fluence that leads to ablation. A total of 16% of the molecules were each given 1.84 eV of kinetic energy in the internal mode. This corresponds to a total energy density of 0.30 eV deposited per matrix molecule within the penetration depth. This deposited energy density is slightly less than the cohesive energy of 0.31 eV of the 2D model organic solid. Three snapshots of the simulation are shown in Figure 3 for model C (4806 matrix and eight analyte molecules). Qualitatively the picture fits with the conventional wisdom of laser ablation. Most but not all of the molecules in the irradiated region are being ablated and the analyte molecules are moving at about the same velocity as the matrix molecules (or conversely, the analyte molecules are not getting left behind). The structure of the ejected plume and the results concerning the analyte molecules will be discussed later in this section. First we shall perform a detailed analysis of the processes in the irradiated material leading to ablation.

The spatial and time development of the internal or vibrational energy of molecules, the local hydrostatic pressure, and the

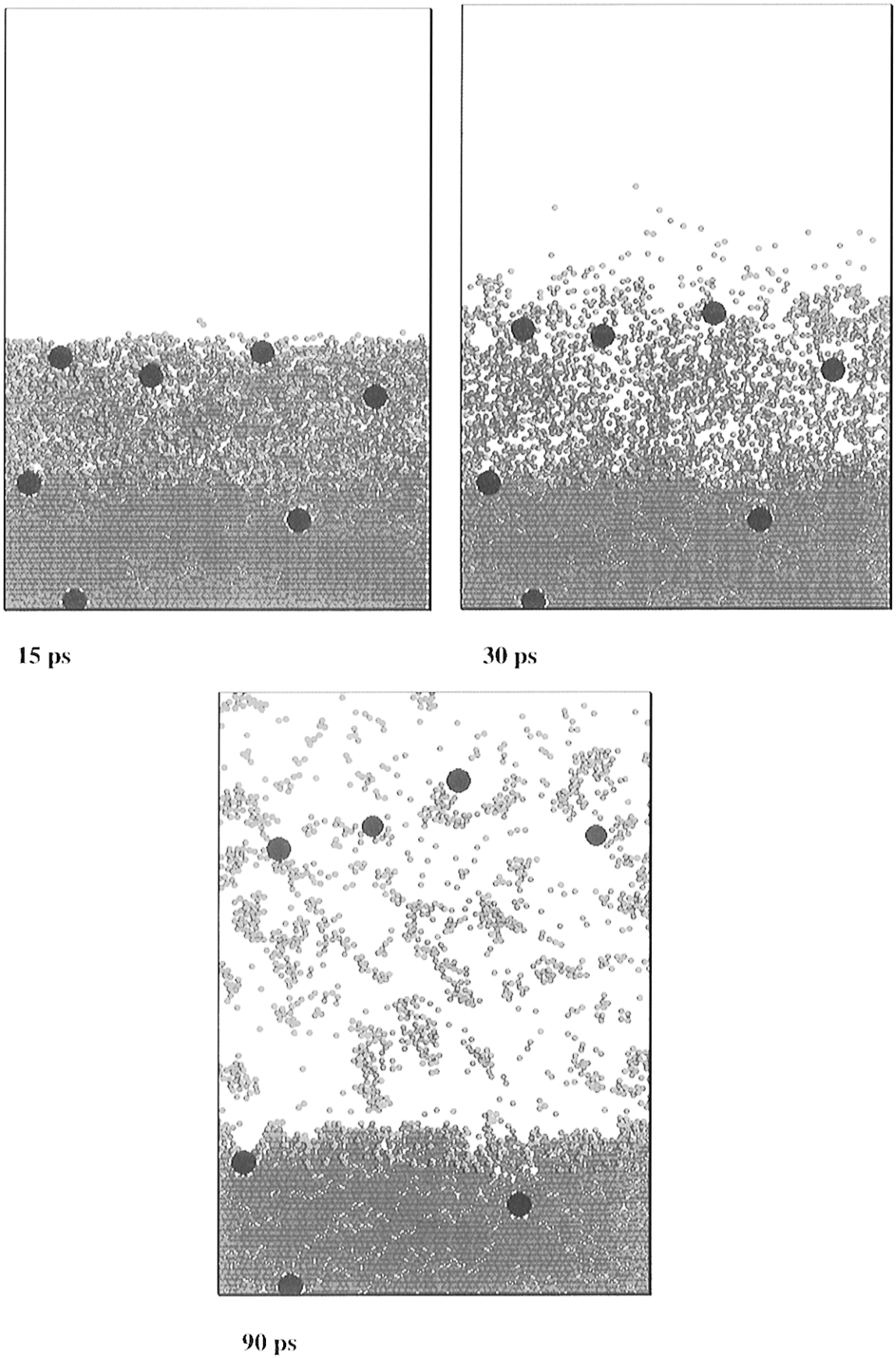

Figure 3. Snapshots from a MD simulation of laser ablation, model C. The blue and red small spheres represent unexcited and excited matrix molecules. The larger green spheres represent analyte molecules.

defect density in the material are presented for model A (58 800 molecules) in the form of contour plots in Figure 4. The model sample is divided into 105 horizontal zones, and contour plots are drawn through the points corresponding to the average of the quantity for all the molecules in the zone. In the case of model A, one zone consists of 560 molecules or four molecular monolayers. In other words, each data point corresponds to the averaging over 560 molecules that are *initially* situated at

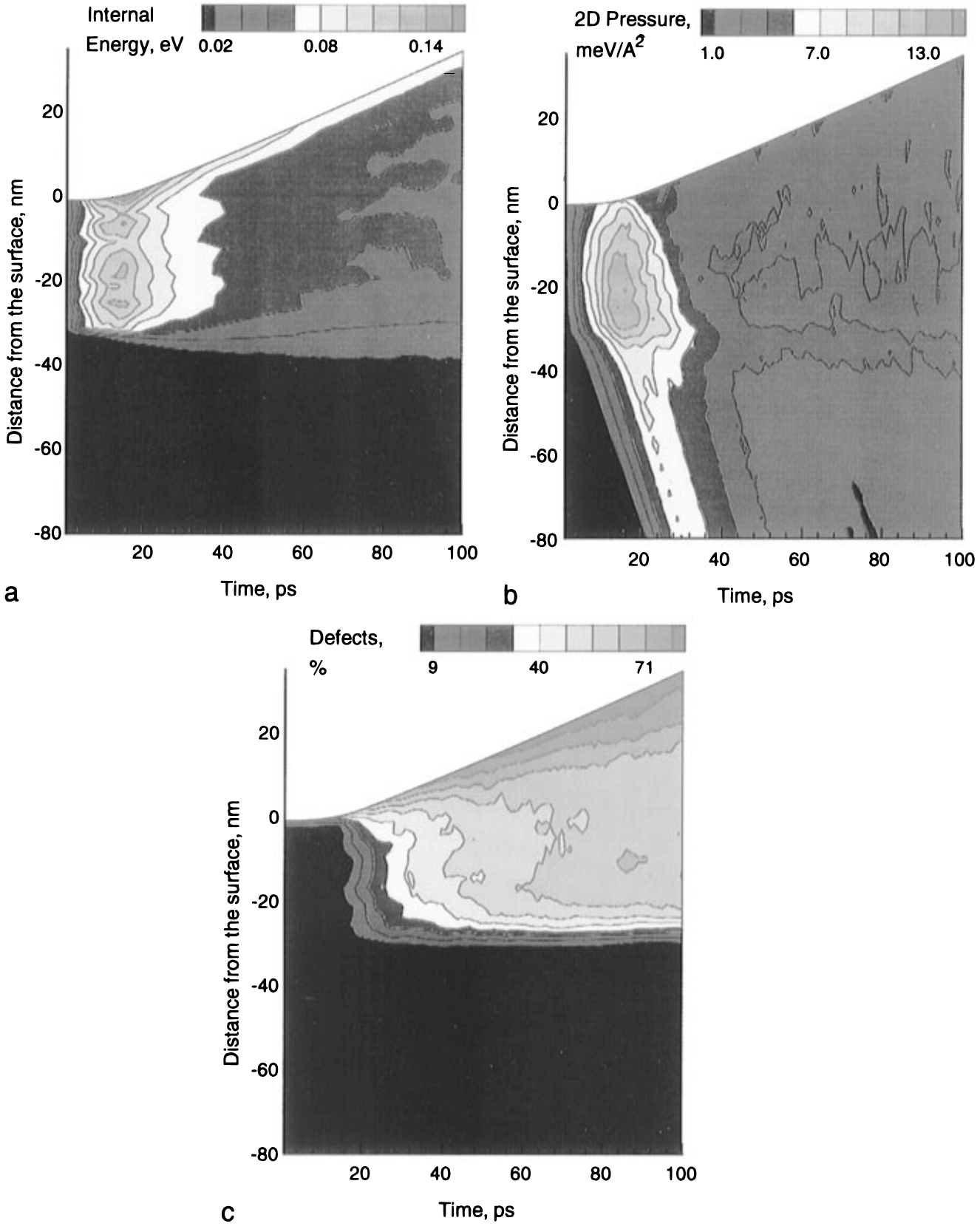

Figure 4. Spatial and time distributions for model A: (a) internal molecular energy; (b) local hydrostatic 2D pressure; (c) defect density. The laser pulse is 15 ps and the penetration depth is 32 nm. The depth shown is 80 nm and the entire sample is 210 nm.

nearly the same depth in the sample. The data points are calculated at 1 ps intervals during the MD trajectories starting from the beginning of a laser pulse. The data for the upper 80 nm of the sample (40 zones) for the first 100 ps of simulation are presented in Figure 4. The abscissa is the average vertical position of each zone; thus the nonrectangular shape of the contour plots reflects the ejection of part of the irradiated volume. The material characteristics averaged over the upper 24 nm (12 zones) are plotted in Figure 5.

Figure 4a shows that the internal energy of molecules within the laser penetration depth increases during the pulse duration due to the laser light absorption. The internal energy then

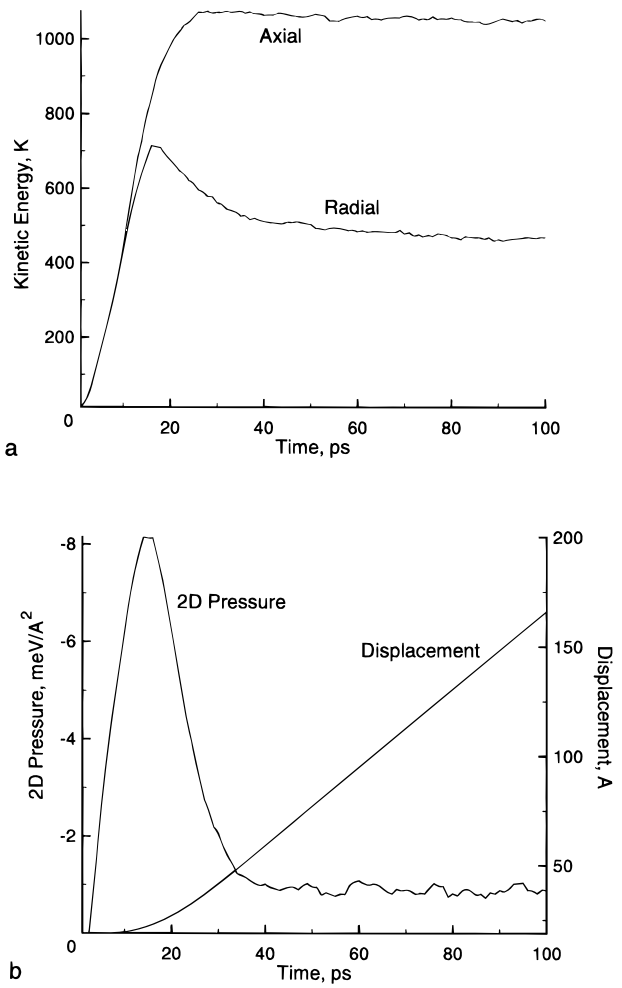

Figure 5. Material characteristics versus time. All quantities are averaged over the molecules in the original top 24 nm of the system. The results are for the 2D simulation shown in Figure 1a. (a) Axial and radial kinetic energies. The kinetic energies are given in Kelvin, but no implications about equilibrium are made. (b) 2D pressure and displacement.

equilibrates with the thermal energy of translational motion of molecules within 10−20 ps. The energy transfer in molecules from the top layers is slower due to fewer intermolecular interactions and ejection of excited molecules that have insufficient time to relax.

The rapid energy transfer from the vibrationally excited molecules results in intensive energy pumping into the thermal energy of the organic crystal and a sharp temperature rise within the laser penetration depth on the time scale of the pulse duration, Figure 5a. The heating rate of the material is faster than the material can undergo thermal expansion, and a high pressure builds up in the irradiated volume, Figures 4b and 5b. This high pressure formed within the penetration depth then relaxes by expansion of the irradiated material. In the direction down from the surface, the relaxation of the laser-induced pressure drives a strong compression wave into the cold part of the sample, Figure 4b. In the opposite direction, the pressure gradient leads to the forces driving the acceleration of the top layers in the direction normal to the surface. That can be seen from Figure 5b, where the average displacement of the upper 24 nm (the biggest part of irradiated volume) is plotted. The acceleration of the region as a whole starts at ∼10 ps, when the pressure reaches a high level, and is over at ∼25 ps, when the pressure drops down. The displacement then increases linearly with time, indicating that the whole region is ablated and moves away from the sample with an *average* velocity of 200 m/s. We find that the velocities of the ejected particles are nonuniformly distributed in the plume, and the momentum transfer from the lower particles to the top particles results in the high, ∼700 m/s, plume-front velocities in the 2D model.

Additional insight into the picture given above of ablation driven by the dynamics of the pressure relaxation comes from examining the thermodynamic and structural characteristics of the ejection process. The melting temperature of the 2D system is found to be about 400 K when melting is simulated by slow heating at zero pressure. The rapid heating of the material exposed to a short laser pulse causes strong compressive pressures, which can suppress the initiation of the melting phase transition up to a high degree of overheating. To have a quantitative description of the structural and phase changes in the model, we monitor development of the defect density distribution, Figure 4c. Except for the shallow surface region, no defects are detected during the most of the 15 ps laser pulse. Only close to the end of the laser pulse, when the average kinetic energy within the penetration depth reaches ∼700 K, Figure 5a, does the defect density start to rise sharply and nearly linearly with time, Figure 4c. During the short time span between 15 and 30 ps the defect density is increasing up to the level that far exceeds the one characteristic of the liquid state. It is noteworthy that this increase starts simultaneously and proceeds with nearly the same rate in the whole irradiate part of the sample. This points to a rapid *homogeneous* phase transition/explosion from a solid directly to a gaseous phase consisting of a mixture of sublimated molecules and molecular clusters. On the basis of thermodynamic considerations, the phase explosion or homogeneous explosive boiling has been indeed predicted to occur under conditions of intensive laser irradiation.[46,47] A more detailed analysis of the nature of the nonequilibrium phase explosion and its connection to the threshold behavior in laser ablation will be given elsewhere.[48]

The phase explosion contributes to buildup of the high pressure in the material despite the quick expansion. In this regard the phase explosion plays the same part as thermochemical processes in the picosecond laser ablation of polymers.[49] Another important consequence of the phase explosion is the fast cooling of the ejected plume due to the adiabatic expansion and intensive disintegration of the matrix.[50] The kinetic energy of thermal motion is tranferred into the potential energy of material disintegration and the flow energy of the ejected plume. The time dependence of the average kinetic energy of molecular motion parallel (radial) and perpendicular (axial) to the surface is shown in Figure 5a. The divergence of the axial and radial kinetic energies starts at 10 ps coincidentally with the laser pressure induced expansion and acceleration, Figure 5b, of irradiated volume. This acceleration is responsible for the sharp increase of the axial kinetic energy, which nearly doubles during the short period of pressure relaxation (10−25 ps). The energy of the material flow out of the surface accounts for the biggest part of this increase of axial kinetic energy. At the same time, the cooling of the expanding material starts to compete with the laser energy pumping into the thermal energy and reduces the rate of the increase of the radial kinetic energy, Figure 5a. The radial kinetic energy then decreases quickly, within 15 ps, Figure 5a. This decrease coincides in time with the phase explosion, Figure 4c, indicating that the cooling is the result of the explosive matrix disintegration. This cooling affects equally the radial and axial kinetic energies. In the case of the axial kinetic energy the cooling competes with the concurrent axial acceleration of the ejected material and is not apparent in Figure 5a. In MALDI, the fast cooling of the ejected plume due to the phase explosion and the short time that analyte molecules

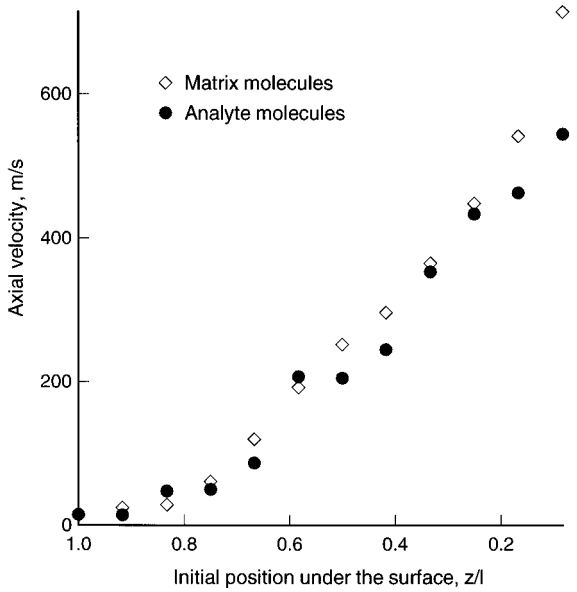

Figure 6. Axial velocities of matrix and analyte molecules at a time of 500 ps as a function of their initial position under the surface, *z*, relative to the laser penetration depth, *l*. The data points correspond to the averaging of the results of five runs for model B.

remain in the energetic environment created by the laser pulse are the conditions that can preserve the analyte molecules intact.[16]

The phase explosion of a metastable overheated liquid results in the ejection of the plume consisting of the molecular clusters or liquid droplets of different sizes along with the individual molecules. The velocities of the ejected clusters and molecules are nonuniformly distributed in the ejected plume. The molecules that originate from the top layers acquire higher axial velocities at early times, ~10−20 ps, after the laser impact. We find that intermolecular collisions in the plume lead to additional changes in the axial energy profile. The axial velocity of the molecules from upper layers continues to increase even after they are ejected high above the surface. This energy and momentum transfer from the lower layers to the top layers results in the high maximum velocities of the plume expansion, Figure 6, and strongly forwarded ejection as observed in MALDI experiments.[6−8,13] As a result of the collective ejection process, the big analyte molecules get axial acceleration from an expanding plume and move along with the matrix molecules at approximately the same velocity, Figure 6. There is a difference in the statistical significance of the points in Figure 6 for matrix and analyte molecules, where each point corresponds to the average velocity of either ~3000 matrix molecules or four to seven analyte molecules.

In contrast to the axial velocities, we find that the radial velocities of the ejected molecules have no significant correlation with the initial position of molecules under the surface. The fast decrease in the radial kinetic energy due to the explosive matrix disintegration discussed above is followed by a much slower gradual cooling of the ejected material down to the melting point. This process has been connected with the cluster decomposition. We find that both processes of the axial energy redistribution and the radial cooling in the plume last longer than the time of our simulation, 1 ns. A more detailed analysis of the processes in the plume and their role in the formation of the final velocities and angle distributions will be given elsewhere.[51]

The preliminary results of the simulation performed on the 3D model agree well with the qualitative scenario for the ablation process outlined above on the basis of the 2D results.

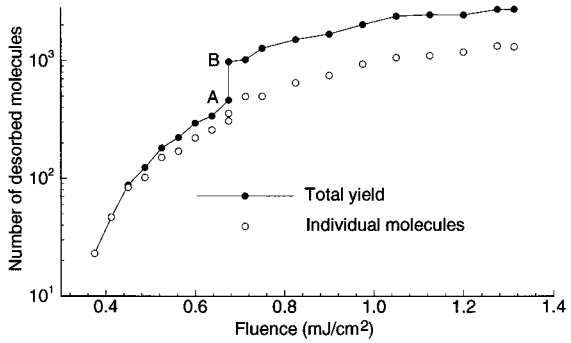

Figure 7. Ablation yield as a function of laser fluence for the 3D model of the molecular solid.

To reproduce a yield−fluence relationship for the 3D model and determine the threshold fluence for the ablation, we have performed a series of simulations at different laser fluences. We find that at a laser fluence of 0.4 mJ/cm^2 a noticeable number of molecules start to desorb from the surface, Figure 7. The yield gradually increases to a fluence of 0.675 mJ/cm^2, point A in Figure 7, where a stepwise increase of the total yield occurs. We have repeated the simulation at 0.675 mJ/cm^2 four times and obtained a total yield of ~500 molecules three times and about 1000 molecules once, points A and B in Figure 7, respectively. Increasing the irradiation dose beyond 0.675 mJ/cm^2 leads to the monotonic increase of the yield with clear evidence of saturation at high fluences. Both the sharp initial increase of the molecular yield and the saturation at high fluences are features typical of experimental results.[5,9,10,14]

The most prominent feature of the calculated curve is the stepwise increase in the total yield at 0.675 mJ/cm^2. This feature clearly breaks the ejection process into two distinct regions. We find that there is a dramatic difference in the plume structure that corresponds to the low- and high-fluence portions of the curve in Figure 7. Primarily single molecules with a small number of molecular dimers and trimers are ejected at fluences lower than 0.675 mJ/cm^2. This indicates that the ejection mechanism at these fluences is an intensive surface vaporization. Starting from point B the ejected plume is found to contain a substantial fraction of large molecular clusters. In particular, the fraction of ejected molecules in clusters composed of 10 or more molecules increases from 2% of the total yield for point A up to 41% for point B and then gradually decreases down to ~20% at highest fluences simulated. This clearly indicates that the mechanism of ejection changes at the fluence of 0.675 mJ/cm^2 from evaporation to the collective ejection process or ablation. Preliminary analysis indicates that the physical picture of the ablation process presented above for the 2D model is valid also for the 3D system.

Comparing the simulation data with experimental mass spectrometry measurements,[3−14] one should take into account the difference between the total yield and the yield of individual particles that are shown in Figure 7. The commonly measured fluence dependence of the yield of individual particles is found to have no step increase at the ablation threshold. This suggests that the experimental threshold for matrix molecules corresponds to a detection threshold[9] in the evaporation regime, whereas the ablation threshold predicted by the model is likely to correspond to the real physical threshold for the ejection of large analyte molecules in MALDI.[5] In this case the observation of Ens et al.[5] that at the threshold fluence either a large number of analyte ions are produced in a *successful* event or none at all can be directly correlated with the existence of *certain probability* for the triggering of the ablation at the threshold in our model.

For quantitative comparisons between the computed and experimental threshold fluences we take into account the fact that the penetration depth used in the 3D model is underestimated by a factor of ~20 compared to the typical UV-MALDI conditions.[3] Thus about 20 times higher fluence would be required to produce a similar distribution of the deposited energy within a realistic penetration depth. This rough estimation gives us an ablation threshold of ~10−20 mJ/cm^2 that reasonably matches the experimental values.[3,5,9,10] We should point out, however, that exact quantitative scale up of the simulation results to experimental conditions is impossible. Different processes that determine the desorption and ablation phenomenon have different dependences on the laser penetration depth and pulse duration. The development of the nonreflecting boundary conditions and parallelization of the MD code should allow us to additionally extend the time and length scales of the model and perform a more justified extrapolation to the typical experimental conditions.

Finally we note that the 3D model predicts higher maximum velocities of the ejected molecules than the ones predicted by the 2D model, Figure 6. The average velocity of the molecules originated from the top layer (that would correspond to the rightmost point in Figure 6 in the case of the 2D model) is found to vary between 600 m/s at the ablation threshold up to 1500 m/s at the highest simulated fluence of 1.3 mJ/cm^2. This result is in good agreement with the reported velocities of the plume expansion.[6−8,13,14]

V. Summary

The relatively long time scale and large number of molecules involved in laser ablation are the factors that have hampered the application of molecular dynamics simulations in this field. To overcome these limitations, we propose a MD model of breathing spheres, a model with true translational and approximate internal degrees of freedom. The main features of the proposed model are as follows:

(i) Experimental parameters such as laser power and wavelength, pulse width, and penetration depth are used to simulate the laser irradiation.

(ii) Microscopic effects of molecular excitation by photon absorption (photochemical reactions, vibrational excitations) are included, and the issue of thermal versus photochemical ablation can be addressed.

(iii) An internal degree of freedom is introduced to reproduce a realistic rate of vibrational relaxation of the excited molecules.

(iv) An approximate representation of the internal molecular motion permits a significant increase in the number of molecules to be treated in the simulation study. Up to 58 800 molecules are included in a computational cell used in the present work.

(v) Several types of molecules can be incorporated into the model to simulate complex organic solids.

(vi) Development of temperature, pressure, and energy distributions in the system can be calculated and compared with experimental data and predictions of analytic models.

The model is applied in this work to the investigation of the laser ablation of molecular systems. The 2D and 3D models are used in concert to sort out the important phenomena and correlate them to experimental conditions and observations. We believe that the model provides a realistic description of the ablation process. In particular, the calculated yields versus fluence dependence has a stepwise increase of molecular yield with increasing fluence and saturation at high fluences. A well-defined threshold fluence has been found to separate two distinct mechanisms for the ejection of molecules, surface vaporization at low laser fluences and collective ejection or ablation at high fluences. A stepwise increase of the yield and a fundamental change in the structure of the ejected plume are predicted to occur at the threshold fluence. Above the threshold the laser-induced high pressure and the explosive homogeneous phase transition from a solid directly to a gaseous phase consisting of mixture of sublimated molecules and molecular clusters lead to the strongly forwarded emission of ablated material and high, from 500 up to 1500 m/s, maximum velocities of the ejected plume expansion. Large molecular clusters are found to constitute a significant part of the ejected plume at fluences close to the ablation threshold.

The model predicts that the processes in the plume significantly influence the final velocities and angle distributions. Intermolecular collisions in the plume lead to the axial energy and momentum transfer from the lower layers to the top layers. This effect can significantly contribute to the high maximum velocity of the plume expansion and large velocity spread observed for matrix molecules in MALDI experiments. At the same time the radial kinetic energy of the ejected molecules is found to have no significant correlation with the initial position of molecules under the surface. The explosive phase transition and matrix disintegration cause a fast decrease in the radial energy. Subsequent plume expansion and cluster decomposition lead to the additional gradual radial cooling of the ejected material.

Large analyte molecules incorporated in the matrix get axial acceleration from an expanding plume and move along with the matrix molecules at nearly the same velocity. The fast cooling of the expanding plume can be an important factor that provides the conditions for the large analyte molecules to survive volatilization.

Acknowledgment. We gratefully acknowledge financial support from the Office of Naval Research through the Medical Free Electron Laser Program and the National Science Foundation. The computational support for this work was provided by the IBM-Selected University Research Program and the Center for Academic Computing at Penn State University. We appreciate helpful discussions with R. Srinivasan, R. F. Haglund, D. Dlott, R. J. Levis, and F. Hillenkamp.

References and Notes

(1) *Proceedings of Laser−Tissue Interaction VII*; Jacques, S. L., Ed.; SPIE Proceedings Series 2681; 1996.

(2) *Methods and Mechanisms of Producing Ions from Large Molecules*; Standing, K. G., Ens, W., Eds.; NATO ASI Series 269; Plenum Press: New York, 1991.

(3) Karas, M. In *Fundamental Processes in Sputtering of Atoms and Molecules (SPUT 92)*; Sigmund, P., Ed.; Det Kongelige Danske Videnskabernes Selskab: Copenhagen, 1993; p 623.

(4) Karas, M. *Biochem. Mass Spectrom.* **1996**, *24*, 897.

(5) Ens, W.; Mao, Y.; Mayer, F.; Standing, K. G. *Rapid Commun. Mass Spectrom.* **1991**, *5*, 117.

(6) Zhou, J.; Ens, W.; Standing, K. G.; Verentchikov, A. *Rapid Commun. Mass Spectrom.* **1992**, *6*, 671.

(7) Beavis, R. C.; Chait, B. T. *Chem. Phys. Lett.* **1991**, *181*, 479.

(8) Pan, Y.; Cotter, R. C. *Org. Mass Spectrom.* **1992**, *27*, 3.

(9) Dreisewerd, K.; Schürenberg, M.; Karas, M.; Hillenkamp, F. *Int. J. Mass Spectrom. Ion Processes* **1995**, *141*, 127.

(10) Dreisewerd, K.; Schürenberg, M.; Karas, M.; Hillenkamp, F. *Int. J. Mass Spectrom. Ion Processes* **1996**, *154*, 171.

(11) Ehring, H.; Sundqvist, B. U. R. *Appl. Surf. Sci.* **1996**, *96−98*, 577.

(12) Berkenkamp, S.; Karas, M.; Hillenkamp, F. *Proc. Natl. Acad. Sci. U.S.A.* **1996**, *93*, 7003.

(13) Preisler, J.; Yeung, E. S. *Appl. Spectrosc.* **1995**, *49*, 1826.

(14) Braun, R.; Hess, P. *J. Chem. Phys.* **1993**, *99*, 8330.

(15) Johnson, R. E. In *Large Ions: Their Vaporization, Detection and Structural Analysis*; Baer, T., Ng. C. Y., Powis, I., Eds.; John Wiley: New York, 1996; p 49.

(16) Vertes, A. In ref 2; p 275.

(17) Vertes, A.; Lavine, R. D. *Chem. Phys. Lett.* **1990**, *171*, 284.

(18) Garrison, B. J.; Srinivasan, R. *J. Appl. Phys.* **1985**, *57*, 2909.

(19) Garrison, B. J.; Srinivasan, R. *Appl. Phys. Lett.* **1984**, *44*, 849.
(20) Bencsura, A.; Vertes, A. *Chem. Phys. Lett.* **1995**, *247*, 142.
(21) Venugopalan, V. In *Proceedings of Laser−Tissue Interaction IV*; Jacques, S. L., Ed.; SPIE Proceedings Series 2391; 1995; p 184.
(22) Itzkan, I.; Albagli, D.; Dark, M. L.; Perelman, L. T.; von Rosenberg, C.; Feld, M. S. *Proc. Natl. Acad. Sci. U.S.A.* **1995**, *92*, 1960.
(23) Bernardo, D. N.; Bhatia, R.; Garrison, G. J. *Comput. Phys. Commun.* **1994**, *80*, 259.
(24) Shiea, J.; Sunner, J. In ref 2; p 147.
(25) Banerjee, S.; Johnson, R. E.; Cui, S.-T.; Cummings, P. T. *Phys. Rev.* **1991**, *B43*, 12707.
(26) Urbassek, H. M.; Kafemann, H.; Johnson, R. E. *Phys. Rev.* **1994**, *B49*, 786.
(27) Fenyö, D.; Johnson, R. E. *Phys. Rev.* **1992**, *B46*, 5090.
(28) Urbassek, H. M.; Waldeer, K. T. *Phys. Rev. Lett.* **1991**, *67*, 105.
(29) Herrmann, R. F. W.; Gerlach, J.; Campbell, E. E. B. *Nucl. Instrum. Meth. Phys. Res. B*, in press.
(30) Kitaigorodsky, A. I. *Molecular Crystals and Molecules*; Academic Press: New York, 1993.
(31) Wyatt, R. E.; Iung, C.; Leforestier, C. *Acc. Chem. Res.* **1995**, *28*, 423.
(32) Kodali, P. B. S.; Garrison, B. J. *J. Chem. Phys.*, submitted.
(33) Chang, T.-C.; Dlott, D. *J. Chem. Phys.* **1989**, *90*, 3590.
(34) Kim, H.; Postlewaite, J. C.; Zyung, T.; Dlott, D. *Appl. Phys. Lett.* **1989**, *54*, 2274.
(35) Zare, R. N.; Levine, R. D. *Chem. Phys. Lett.* **1987**, *136*, 593.
(36) Zhigilei, L. V.; Srivastava, D.; Garrison, B. J. *Surf. Sci.*, in press.
(37) Likhachev, V. A.; Mikhailin, A. I.; Zhigilei, L. V. *Philos. Mag. A* **1994**, *69*, 421.
(38) Gilath, I. In *High-Pressure Shock Compression of Solids II. Dynamic Fracture and Fragmentation*; Davison, L., Grady, D. E., Shahinpoor, M., Eds.; Springer-Verlag: New York, 1996; p 90.
(39) Trucano, T.; McGlaun, J. M.; Farnsworth, A. In *Proceedings of Laser−Tissue Interaction V*; Jacques, S. L., Ed.; SPIE Proceedings Series 2134A; 1994; p 179.
(40) Boslough, M. P.; Assay, J. R. In *High-Pressure Shock Compression of Solids*; Asay, J. R., Shahinpoor, M., Eds.; Springer-Verlag: New York, 1993; p 7.
(41) McTague, J. P.; Frenkel, D.; Allen, M. P. In *Ordering in Two Dimensions*; Sinha, S. K., Ed.; North-Holland: Amsterdam, 1980; p 147.
(42) Fisher, D. S.; Halperin, B. I.; Morf, R. *Phys. Rev. B* **1979**, *20*, 4692.
(43) Nelson, D. R. *Phys. Rev. B* **1983**, *28*, 5515.
(44) Vitek, V.; Egami, T. *Phys. Status Solidi B* **1987**, *144*, 145.
(45) Nordsieck, A. *Math. Comput.* **1962**, *16*, 22.
(46) Martynyuk, M. M. *Sov. Phys. Tech. Phys.* **1976**, *21*, 430.
(47) Kelly, R.; Miotello, A. *Appl. Surf. Sci.* **1996**, *96−98*, 205.
(48) Zhigilei, L. V.; Kodali, P. B. S.; Garrison, B. J. *Phys. Rev. Lett.*, submitted.
(49) Hare, D. E.; Franken, J.; Dlott, D. D. *J. Appl. Phys.* **1995**, *77*, 5950.
(50) Sunner, J.; Ikonomou, M. G.; Kebarle, P. *Int. J. Mass Spectruom. Ion Processes* **1988**, *82*, 221.
(51) Zhigilei, L. V.; Garrison, B. J. In preparation.